

# Impact of initial pulse shape on the nonlinear spectral compression in optical fibre

Sonia Boscolo <sup>1</sup>, Frederic Chaussard <sup>2</sup>, Esben Andresen <sup>3</sup>,

Hervé Rigneault <sup>4</sup> and Christophe Finot <sup>2,\*</sup>

<sup>1</sup> *Aston Institute of Photonic Technologies, School of Engineering and Applied Science, Aston University, Birmingham B4 7ET, United Kingdom*

<sup>2</sup> *Laboratoire Interdisciplinaire Carnot de Bourgogne, UMR 6303 CNRS-Université de Bourgogne-Franche-Comté, 9 avenue Alain Savary, BP 47870, 21078 Dijon Cedex, France*

<sup>3</sup> *Univ. Lille, CNRS, UMR 8523 – PhLAM – Physique des Lasers Atomes et Molecules, F-59000 Lille, France*

<sup>4</sup> *Institut Fresnel, CNRS, Aix-Marseille Université, Ecole Centrale Marseille, Campus de Saint Jérôme, F-13397 Marseille Cedex 20, France*

*\* Corresponding author:*

*E-mail address: [christophe.finot@u-bourgogne.fr](mailto:christophe.finot@u-bourgogne.fr)*

*Tel.: +33 3 80395926*

**Abstract:** We theoretically study the effects of the temporal intensity profile of the initial pulse on the nonlinear spectral compression process arising from nonlinear propagation in an optical fibre. Various linearly chirped input pulse profiles are considered, and their dynamics is explained with the aid of time-frequency representations. While initially parabolic-shaped pulses show enhanced spectral compression compared to Gaussian pulses, no significant spectral narrowing occurs when initially super-Gaussian pulses are used. Triangular pulses lead to a spectral interference phenomenon similar to the Fresnel bi-prism experiment.

© 2017 Elsevier. Licensed under CC BY NC ND.

Keywords: Nonlinear spectral compression; nonlinear fiber optics; pulse shaping

# 1. Introduction

Self-phase modulation (SPM) in optical fibre is ordinarily associated with spectral broadening of an ultra-short optical pulse. However, for appropriate initial conditions of the input pulse, SPM can result in significant spectral compression [1]. Indeed, SPM causes spectral compression or broadening depending on the initial frequency modulation (chirp) of the pulse electric field. Specifically, a pulse with a negative chirp, such as that imparted by an anomalously dispersive element, is compressed by the effects of SPM [2-4]. This method of spectral compression has been implemented using various types of fibres [5-8] and has also been studied in nonlinear waveguides [9]. It is suitable for a very large range of wavelengths including Ti:sapphire wavelengths [5, 8], the widely used 1- $\mu\text{m}$  [7, 10, 11] and 1.55- $\mu\text{m}$  [12] windows and the emerging 2- $\mu\text{m}$  band [13]. The process can also sustain simultaneous amplification of the pulse [10, 11, 13, 14], thereby providing an attractive solution to convert ultra-short pulses delivered by femtosecond oscillators into high-power, near-transform-limited picosecond pulses, and to counteract the spectrum expansion that usually occurs with the direct amplification of picosecond structures.

Most of the theoretical and experimental works to date have considered usual initial pulse profiles such as Gaussian or hyperbolic secant pulses [3, 5, 8, 10, 11, 14]. However, several recent studies have demonstrated that the use of pre-shaped input pulses with a parabolic waveform can achieve spectral compression to the Fourier transform limit owing to the fact that for such pulses the cancellation of the linear and nonlinear phases can be made complete [15-17]. The purpose of this paper is to provide insight into the influence of the input temporal intensity profile on the spectral dynamics of negatively chirped pulses that occurs upon nonlinear propagation in a fibre. In particular, we emphasize that spectral narrowing does not occur for any initial pulse shape, and that there are significant differences between the propagation of parabolic, Gaussian, super-Gaussian or triangular pulses, which we elucidate with the aid of a time-frequency analysis. We show that initially parabolic-shaped pulses provide the best results in terms of quality of the compressed spectrum. Initially Gaussian pulses undergo efficient spectral compression, but the resulting spectrum exhibits residual pedestals stemming from uncompensated higher-order phase. On the contrary, super-Gaussian pulses do not experience any spectral narrowing, and their spectral extent does not change significantly upon propagation. In the case of triangular pulses, we observe a spectral interference phenomenon similar to Fresnel bi-prism interference. Simple analytic formulae are presented, which can predict the evolution of the spectral extent of the

different input pulses along the fibre. We also discuss the impact of realistic initial conditions and system parameters on the spectral dynamics, and show that the interference pattern observed with triangular pulses is strongly affected by deviations of the initial waveform from the ideal shape.

## 2. Ideal nonlinear propagation of differently shaped pulses

### Situation under investigation

In this section, we study the propagation in a nonlinear optical fibre of initially perfect pulse waveforms with a negative linear chirp, given by  $\psi_{in}(t) = \sqrt{P I_{in}(t)} \exp(-i A t^2 / 2)$ . Here,  $I_{in}(t)$  is the temporal intensity profile of the pulse,  $P$  is the pulse peak power, and  $A$  is the chirp coefficient. We assume that these pulses have been temporally stretched in an anomalously dispersive medium so as to acquire a parabolic temporal phase over far-field evolution. For the purpose of illustration, we consider pulses at the wavelength 1550 nm, with a full-width at half maximum (FWHM) duration  $T_{fwhm} = 100$  ps (after dispersive temporal broadening) and  $A = -16.7 \cdot 10^{-3} \text{ rad.ps}^{-2}$ , yielding a spectral FWHM bandwidth  $\Omega_{fwhm,0} \approx |A| / T_{fwhm}$  in the far-field regime. Four ideal and symmetric pulse shapes are investigated: a parabolic pulse with  $I_P(t) = (1 - t^2 / T_P^2) \theta(T_P - |t|)$ , a Gaussian pulse with  $I_G(t) = \exp(-t^2 / T_G^2)$ , a fourth-order super-Gaussian pulse approaching rectangular shape with  $I_S(t) = \exp(-t^8 / T_S^8)$ , and a triangular waveform where  $I_T(t) = (1 - |t| / T_T) \theta(T_T - |t|)$ . Here,  $\theta(x)$  is the Heaviside function. The characteristic temporal values  $T_P$ ,  $T_G$ ,  $T_S$  and  $T_T$  can be related to the FWHM pulse duration as  $T_P = T_{fwhm} / \sqrt{2}$ ,  $T_G = T_{fwhm} / 2\sqrt{\ln 2}$ ,  $T_S = T_{fwhm} / 2(\ln 2)^{1/8}$ , and  $T_T = T_{fwhm}$ . The peak power is set to 12.5 W for the parabolic, Gaussian and super-Gaussian pulses and to 40 W for the triangular pulse. Figure 1 shows the temporal and spectral intensity profiles of the initial pulses.

Our numerical simulations of pulse propagation in the fibre are based on the standard nonlinear Schrödinger equation (NLSE) for the pulse envelope [18]:

$$i \partial_z \psi + \gamma |\psi|^2 \psi - \beta_2 \partial_{tt} \psi / 2 = 0 \quad (1)$$

where  $z$  is the propagation distance,  $t$  is the reduced time,  $\beta_2$  is the group-velocity dispersion (GVD) parameter, and  $\gamma$  is the coefficient of cubic nonlinearity of the fibre. This equation neglects the

effect of fibre loss, as well as higher-order linear and nonlinear effects. Although these effects can have noticeable impact on pulses shorter than 1ps, here we neglect them as the leading-order behavior is well approximated by Eq. (1). We consider here a 500m-long highly nonlinear fibre (HNLF) with the Kerr coefficient  $\gamma = 10 \text{ W}^{-1} \text{ km}^{-1}$  and a low GVD coefficient of  $\beta_2 = 1 \text{ ps}^2 \text{ km}^{-1}$ . With such parameters that are typical of various demonstrations of spectral compression due to SPM in fibre [12], the nonlinearity-dominant regime of propagation is applicable [17]. In this regime, the dispersion term in Eq. (1) plays a relatively minor role and can be neglected. Accordingly, the temporal intensity profile of the pulse does not change along the fibre length, whereas SPM gives rise to a chirp  $\delta\omega_{NL}(t)$  proportional to the temporal gradient of the intensity profile, so that after a propagated distance  $z$ ,  $\delta\omega_{NL}(z,t) = -\gamma P z \partial_t I_{in}$ . The temporal gradients of the various pulse intensity profiles are plotted in Fig. 1(a2). Note that the nonlinear propagation problem being studied can be conveniently normalized by introducing a normalized distance through the nonlinear length  $l / \gamma P$  associated with the pulse at the entrance of the fibre [17, 18]. The resulting temporal chirp of the pulse thus evolves longitudinally as  $\delta\omega(t,z) = A t + \delta\omega_{NL}(z,t) = A t - \gamma P z \partial_t I_{in}$ , which translates in the frequency domain to a modification of the pulse spectrum. The illustration of the impact of the pulse shape on these changes in the spectrum lies at the heart of the present study.

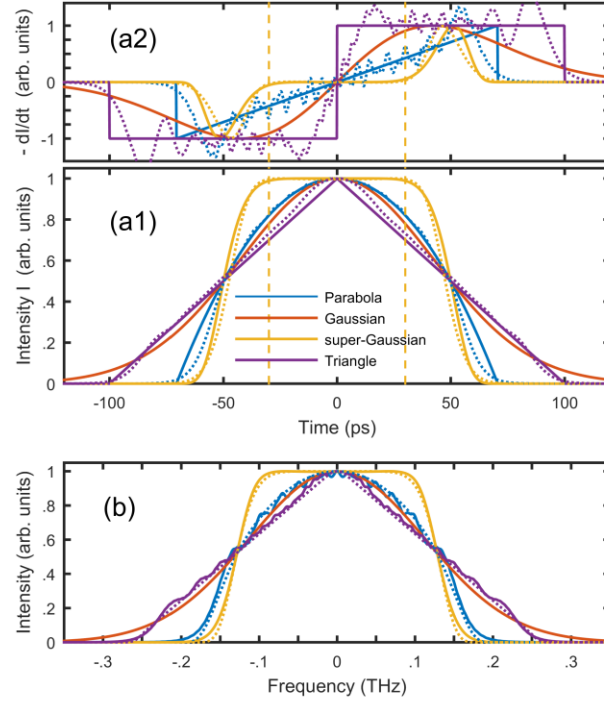


**Figure 1:** (a) Temporal intensity profiles (subplot 1) and temporal intensity gradients (subplot 2), and (b) spectral intensity profiles of parabolic (blue), Gaussian (red), fourth-order super-Gaussian (orange) and triangular (violet) pulses at the entrance of the fibre. The ideal waveforms are plotted with solid lines while the results obtained through frequency-to-time shaping (see section 4) are plotted with dotted lines. The vertical orange dashed lines in panels a delimit the region where the intensity distribution of the super-Gaussian pulse can be reasonably considered as flat.

## Longitudinal evolution of the pulse spectra

First we look into the evolution of the spectra of the different incident pulses in the HNLF. Figure 2 summarizes the results and highlights striking differences among the various evolutions. The spectra of the parabolic and Gaussian pulses undergo significant narrowing in the fibre (panels (a) and (b)), and subsequently re-broaden with further propagation. The super-Gaussian and triangular pulses exhibit very different spectral dynamics and do not experience appreciable spectral compression. The extent of the central part of the spectrum of the super-Gaussian pulse does not change much over the fibre length. On the contrary, the spectrum of the triangular pulse shows strong oscillations before splitting into two symmetric parts that move away from each other during propagation.

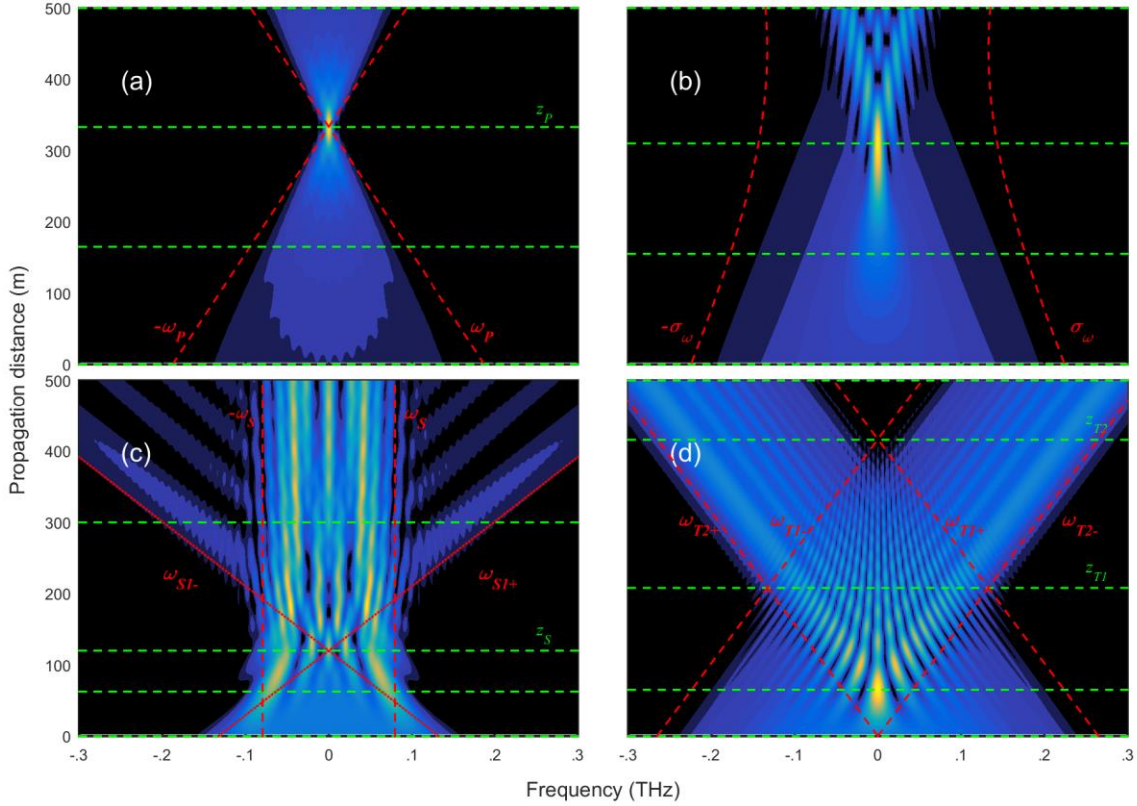


**Figure 2:** Longitudinal evolution of the spectra of ideal (a) parabolic, (b) Gaussian, (c) fourth-order super-Gaussian, and (d) triangular incident pulses. The green dashed horizontal lines indicate the various distances at which the spectrograms of Figs. 4, 5, 6, 7 are taken. The red dashed and dotted lines represent analytical predictions based on a simplified approach.

The very different behavior of the various waveforms is also reflected in Fig. 3, where we plotted the longitudinal evolution of the spectral brilliance of the pulse at its central frequency (panel (a)) and of the Strehl ratio (panel (b)), defined as the ratio of the spectral peak power of the actual pulse and the spectral peak power obtained assuming a flat temporal phase of the pulse [12, 19, 20]. It is seen that the parabolic waveform leads to optimum spectral compression, with the spectral brilliance featuring more than thirty-fold increase with respect to the value at the fiber entrance after a propagation distance  $z_P = 334$  m. The Strehl ratio reaches 1 at  $z_P$ , which pinpoints a Fourier transform-limited pulse. The spectral compression performance is degraded for the Gaussian waveform, which achieves a fourteen-fold enhancement in spectral brilliance at the propagation distance  $z_G = 310$  m. The maximum Strehl ratio is 0.24 for this pulse shape, indicating an imperfect compression where the presence of uncompensated temporal chirp of the pulse leads to the

appearance of side lobes in the pulse spectrum [12, 17]. On the contrary, the spectral brilliances of the triangular and super-Gaussian pulses do not rise greater than five times their initial values, showing that these waveforms do not undergo efficient spectral compression. The corresponding Strehl ratios are very far from optimum values, highlighting the highly chirped nature of the waveforms. These results are confirmed by the evolution of the spectral compression ratio  $C_{rms}$  (panel (c)), defined in terms of root-mean-square (rms) spectral width of the pulse: while  $C_{rms}$  attains a value well above 10 for the parabolic pulse, it does not exceed 2 for the other waveforms being studied.

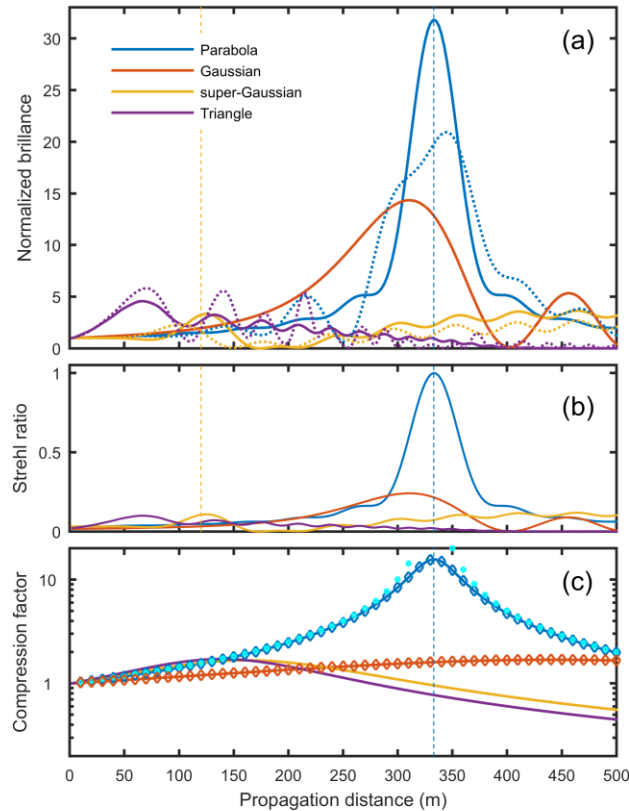


**Figure 3:** Longitudinal evolution of (a) the spectral brilliance at the central frequency, (b) the Strehl ratio, and (c) the rms spectral width for parabolic, Gaussian, fourth-order super-Gaussian and triangular incident pulses (the same color code as in Fig. 1 is used). The dotted curves in subplot (a) represent the results obtained with non-ideal input waves (see section 4). The blue diamonds and cyan circles in subplot (c) represent the results of a theoretical fit to the evolution of the parabolic pulse properties and the predictions from an approximate analytical model, respectively. The orange diamonds in subplot (c) represent the results of the exact analytical calculation of the rms spectral width

given in the Appendix and based on Ref. [21]. The dashed vertical lines indicate the distances  $z_S$  and  $z_P$  of maximum Strehl ratio for the super-Gaussian and parabolic pulses, respectively.

### 3. Nonlinear dynamics of the various pulse waveforms

We now illustrate the observed spectral dynamics of the nonlinear propagation of the various input pulse waveforms in the fibre based on a time-frequency representation of the pulses [22, 23]. Indeed, the use of spectrograms (such as those that can be recorded with cross-correlation frequency-resolved optical gating devices [24]) enables us to provide some simple and intuitive, approximate analytical laws to describe the dynamics. Owing to the linear initial chirp, the common initial state for all waveforms features a distribution of the pulse energy along a line with the negative slope coefficient  $A$ .

#### Parabolic and Gaussian shapes

We first describe the dynamics experienced by an incident parabolic pulse in the fibre (Fig. 4). This is a textbook example to understand the process of spectral compression by SPM and has been already the subject of several investigations [7, 12, 15, 25]. The temporal gradient of the initial pulse intensity profile (indicated by white arrows in Fig. 4(a1)) provides the rate at which the instantaneous frequency of the pulse evolves along the fibre,  $\partial_z \delta\omega_{NL}$ . In the case of an inverted parabola, the chirp generated by SPM has a perfectly linear temporal variation:  $\delta\omega_{NL}(t,z) = 2 \gamma P z t / T_P^2$ . Hence, the temporal variation of the overall chirp of the pulse remains linear upon propagation, with a slope coefficient continuously increasing from negative to positive values:  $C_P(z) = A + 2 \gamma P z / T_P^2$ . The slope coefficient becomes zero at the propagation distance  $z_P = -A T_P^2 / 2 \gamma P$ , hence the pulse is transform-limited (i.e. the Strehl ratio equals 1) at such distance, and the pulse spectrum is significantly narrowed (Fig. 4(b3)) with negligible pedestals – notice that the Fourier transform of a parabolic pulse is a first-order Bessel function of the first kind (sinc-like shape) [16]. Further, the monotonic temporal variation of the chirp at any distance in the fibre inhibits the development of noticeable oscillations in the spectrum, which would otherwise result from interference between different pulse parts having the same instantaneous frequency. We note that for a linearly chirped parabolic pulse with a relatively large chirp coefficient, the temporal shape is imaged in the spectral domain. This can be explained using the stationary phase method, i.e., the cancellation of oscillating contributions with rapidly varying phase. The zero-crossing spectral (half) width can be then evaluated by  $\omega_P = |C_P| T_P$ . The optical spectra in Fig. 4(b) as

well as the results plotted with red dashed lines in Fig. 2(a) show the excellent agreement of the pulse spectral extent foretold by this formula with the results of numerical simulations. The fact that the parabolic pulse spectrum preserves a compact nature with very reduced wings along propagation in the fibre makes it possible for the large rms spectral narrowing shown in Fig. 3(c). It is also apparent from Figs. 3 and 4 that the spectral evolution of the parabolic pulse is perfectly symmetric with respect to the point  $z_P$  of spectral focusing [7]. Based on the above considerations, the evolution of the spectral compression ratio of the pulse can be estimated by using the formula:  $A / |C_P(z)| = 1 / (1 + 2 \gamma P z / A T_P^2)$  (cyan circles in Fig. 3(c)). However, this function clearly diverges as  $z$  approaches  $z_P$ ; accordingly, it overestimates the value of the compression ratio in the vicinity of  $z_P$ . A more accurate description of the evolution of the compression ratio can be obtained by drawing an analogy between the linear chirp generated by the SPM of a parabolic pulse in the temporal domain and the linear chirp imparted onto a pulse by GVD in the spectral domain [7, 12, 16]. Indeed, based on the existing literature on dispersive pulse propagation, we can say that the evolution of the rms spectral width of a parabolic pulse is described by the square root of a non-trivial second-order polynomial [26]. Figure 3(c) highlights the outstanding agreement between this theoretical prediction (blue diamonds) and the numerical simulation results.

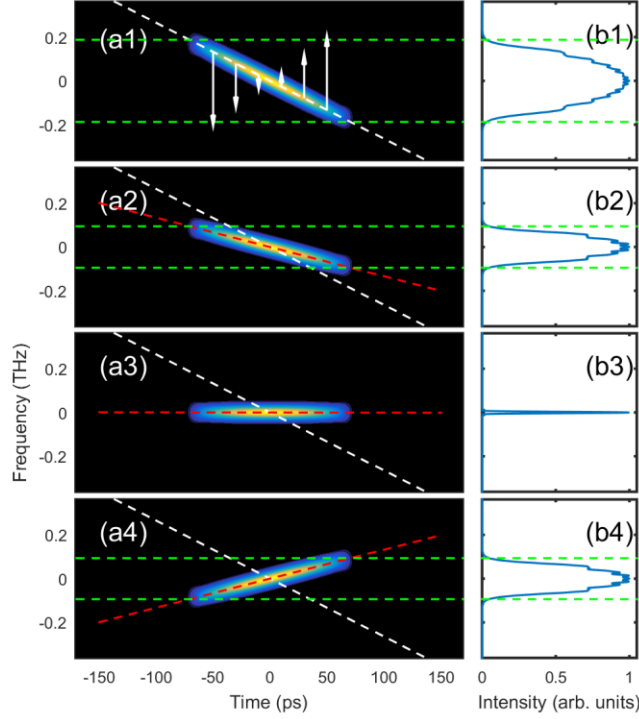


**Figure 4:** Spectro-temporal representation of a parabolic pulse at different propagation distances in the fibre:  $z = 0$ ,  $z = 165$  m,  $z = z_P$ , and  $z = 500$  m (panels 1 to 4, respectively). Subplots (a) and (b) show the spectrograms and the spectral intensity profiles, respectively. The white dashed lines represent the slope coefficient of the pulse chirp at the fibre input  $C_P(0)$ , while the slope coefficients  $C_P(z)$  at the particular nonzero  $z$  are plotted with red dashed lines. The green dashed lines indicate the zero-crossing points of the pulse spectrum  $\pm\omega_P$  as obtained by assuming a strictly parabolic shape of the spectrum. The white arrows have a length proportional to the temporal gradient of the pulse intensity profile.

Next we discuss the dynamics of a Gaussian pulse propagating in the fibre, which are representative of those experienced by waveforms that can be approximated by a parabola in the central part of the pulse. We have indeed confirmed that similar observations can be made in the case of hyperbolic secant or sinusoidal-like waveforms. The linear part of the SPM-induced chirp stemming from a Taylor series expansion of the Gaussian function of the pulse profile about the pulse center to  $O(t^2)$  describes well the actual chirp variation over a large central region of the pulse. Correspondingly, the slope of the central part of the overall chirp evolves in a similar fashion

to the parabolic pulse case:  $C_G(z) = A + 2 \gamma P z / T_G^2$ . However, the deviations from linearity of the chirp generated by SPM in the pulse edges are responsible for several differences between the Gaussian and parabolic spectral dynamics, which can be elucidated with the aid of the spectrograms shown in Fig. 5. We can first notice that as the influence of SPM on the low-intensity wings of the pulse is small, the small portion of energy contained in the wings is not redistributed towards the center of the spectrum. Consequently, while the central part of the spectrum experiences significant and continuous narrowing during an initial stage of evolution, the overall extent of the spectrum does not change appreciably over the fibre length (panels (b)). This explains why the rms spectral compression factor reaches only moderate values in spite of a large increase in brilliance of the central region of the spectrum (Fig. 3). It is noteworthy that the propagation distance at which  $C_{rms}$  is maximal ( $z_s = 440$  m) significantly differs from the distance  $z_G$  of optimum compression in terms of Strehl ratio. The exact formula for the rms spectral width of the pulse derived in the Appendix shows that  $C_{rms}$  cannot exceed the value 1.69 even for very high values of the initial chirp coefficient  $A$ . In light of these observations, we can conclude that the rms compression factor does not provide a good metric to quantify the narrowing of a Gaussian pulse spectrum.

During the initial stage of spectral compression, the chirp has a monotonic temporal variation across the pulse so that no interference effects are observed in the compressed spectrum (Fig. 5(b2)). The chirp becomes zero in the central part of the pulse (i.e.  $C_G = 0$ ) at the propagation distance  $- A T_G^2 / 2 \gamma P = 240$  m. However this distance does not correspond to the optimum compression point  $z_G$ : shortly after this distance, the chirp develops a non-monotonic temporal variation that leads to interference between different pulse parts having the same frequency. Such a constructive interaction has a beneficial impact on the spectral compression process as it contributes to further narrowing of the spectrum and increase of the Strehl ratio, but this comes at the expense of an oscillatory structure of the spectrum (Fig. 5(b3)) [17]. For propagation in the fibre beyond  $z_G$ , as a result of the increase of the chirp slope near the pulse center, the spectrum broadens and the range of frequencies that can interfere becomes larger, thereby leading to the buildup of strong and detrimental oscillations in the pulse wings together with strong side lobes in the resulting spectrum (Fig. 2(b) and panels 4 of Fig. 5).

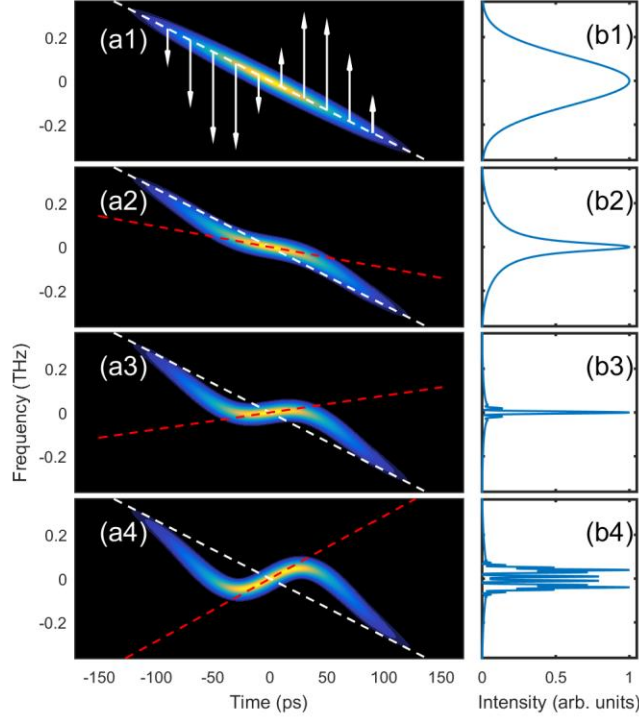


**Figure 5:** Spectro-temporal representation of a Gaussian pulse at different propagation distances in the fibre:  $z = 0$ ,  $z = 93$  m,  $z = z_G$ , and  $z = 500$  m (panels 1 to 4, respectively). Subplots (a) and (b) show the spectrograms and the spectral intensity profiles, respectively. The white dashed lines represent the slope of the chirp in the central part of the pulse at the fibre input  $C_G(0)$ , while the slope coefficients  $C_G(z)$  at the particular nonzero  $z$  are plotted with red dashed lines. The white arrows have a length proportional to the temporal gradient of the pulse intensity profile.

## Super-Gaussian shape

Now we explain why the nonlinear dynamics experienced by an incident super-Gaussian pulse in the fibre does not show any significant spectral compression. When considering the temporal chirp generated by SPM of a super-Gaussian pulse (Fig. 1(b)), we may notice that contrary to a parabolic or a Gaussian pulse, SPM will only induce a chirp in the steep edges of the pulse. Indeed, as the central part of the pulse is almost flat, i.e. it has a very low temporal gradient it will not contribute to create new frequencies in the pulse. Consequently, the main changes during propagation occur in the temporal wings of the pulse, where the energy is redistributed towards the lower frequencies, as it can be observed in Fig. 6. During an initial propagation stage (panels 2), this energy redistribution produces oscillations in the outer region of the temporal plateau of the pulse and,

concomitantly, large spikes appear in the pulse spectrum, which thus develops a ‘batman’-like shape. Then, as the chirp develops further, the spectral region in which interference occurs progressively extends to the whole spectrum. At the propagation distance  $z = 125$  m (panels 3), the energy initially contained in the pulse edges is pushed towards the central frequency, hence the rms spectral width of the pulse is at its minimum. For longer propagation in the fibre (panels 4), the chirp induced in the edges of the pulse becomes larger than the initial extent of the spectrum, thus engendering the development of side lobes in the spectrum. As the new frequencies so generated do not interfere with any other parts of the pulse, these side lobes are free from interference patterns.

We can derive simple rules to characterize these dynamics. If we assume that the plateau of the super-Gaussian waveform (where the SPM is negligible) extends between  $\pm 30\%$  of the FWHM duration, then the initial chirp profile will remain unchanged in this region, which in turn will result into a spectral breadth between  $\pm \omega_S$ , where  $\omega_S = 0.3 |A| / T_{fwhm}$ . These frequencies will represent the boundaries of the region of spectrum where most of the energy is present (red dashed lines Fig. 2(c) and green dashed lines in Fig. 6). Further, if we estimate that the temporal gradient of the pulse profile is achieved at a time position close to half of the FWHM pulse duration, we can then evaluate the total chirp of the pulse by  $\omega_{S1\pm} = \pm A T_{fwhm} / 2 \pm 8 \gamma P z (T_{fwhm} / 2)^7 I_S(t = T_{fwhm} / 2) / T_S^8$ . The predictions provided by this simple formula are in qualitative agreement with the results of numerical simulations (dotted red lines in Fig. 2(c) and dotted green lines in panels 4 of Fig. 6), and explain the linear longitudinal evolution of the side lobes that are generated in the pulse spectrum. For propagation distances  $z < z_{S1}$ , where  $z_{S1}$  can be estimated as the distance where  $\omega_{S1+} = \omega_{S1-} = 0$ , i.e.,  $z_{S1} \approx 120$  m, interference phenomena do not affect the whole central region of the spectrum but are limited to frequencies above  $\omega_{S1-}$  or below  $\omega_{S1+}$ . Shortly after  $z_{S1}$ , the interference occurring at the central frequency engenders an increase of the rms spectral compression factor. For distances  $z > z_{S2}$ , where  $z_{S2}$  can be estimated as the distance where  $\pm \omega_S = \omega_{S1\pm}$ , i.e.  $z_{S2} \approx 192$  m, side lobes appear in the spectrum and, accordingly, the rms compression ratio progressively decreases to values below 1 (Fig. 3(c)).

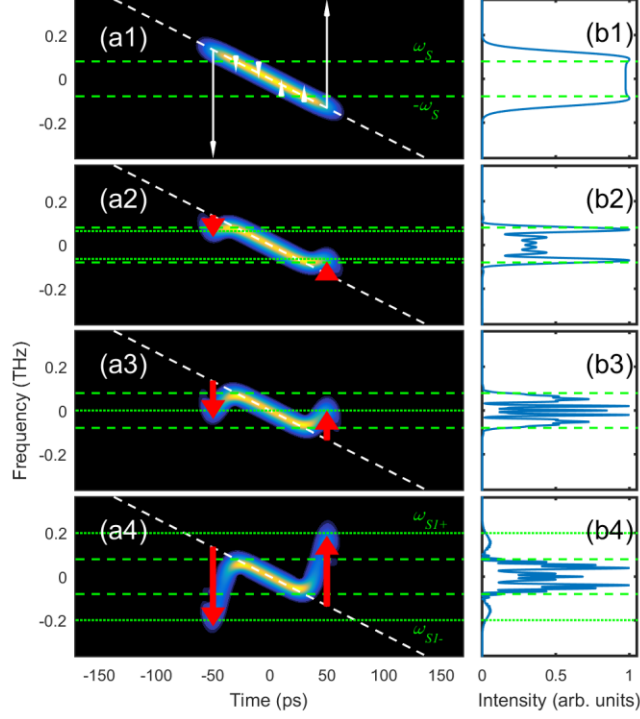


**Figure 6:** Spectro-temporal representation of a fourth-order super-Gaussian pulse at different propagation distances in the fibre:  $z = 0$ ,  $z = 62$  m,  $z = z_{SI}$ , and  $z = 300$  m (panels 1 to 4, respectively). Subplots (a) and (b) show the spectrograms and the spectral intensity profiles, respectively. The white dashed lines represent the slope coefficient of the pulse chirp at the fibre input. The green dashed and dotted lines represent the theoretical predictions for  $\pm\omega_S$  and  $\omega_{ST\pm}$ , respectively. The white arrows have a length proportional to the temporal gradient of the pulse intensity profile. The red arrows represent the frequency shift at  $t = T_{fwhm}/2$ .

## Triangular shape

The observed spectral dynamics for an initial triangular pulse (Fig. 2(d)) are very different from the previously studied cases: after an initial stage of spectral narrowing in which strong oscillations appear in the spectrum, the spectrum splits symmetrically into two parts whose frequency spacing increases linearly over the fibre length. Once again, a spatio-temporal representation of the pulse provides a pedagogical way to visualize and understand these spectral dynamics. Indeed, the temporal intensity profile of a triangular pulse has a constant gradient, which translates into a constant and distinct (opposite sign) frequency chirp induced by SPM onto the leading (down-shifted) and trailing (up-shifted) edges of the pulse:  $\mp\gamma P z / T_T$ , so that the overall chirp of the

pulse evolves according to  $\delta\omega_T(t,z) = A t \pm \gamma P z / T_T$ . We can therefore estimate the frequency boundaries  $\omega_{T1}$  and  $\omega_{T2}$  of each half of the pulse as  $\omega_{T1\pm} = \pm(A T_T + \gamma P z / T_T)$  and  $\omega_{T2\pm} = \pm \gamma P z / T_T$  (the subscripts + and – being used for the leading and trailing edges, respectively).

The different stages of spectral evolution are illustrated in Fig. 7. During an initial stage, the interference that develops in the pulse region containing most of the energy results into strong oscillations in the central part of the spectrum. Then, at the distance  $z_{T1} = -A T_T^2 / 2 \gamma P$  where  $\omega_{T1-} = \omega_{T2+} = -A T_T / 2$  (panels 2), the leading and trailing edges of the pulse overlap and the extent of the spectrum is reduced approximately twofold. At this distance, the spectrum exhibits very fast oscillations with a spectral interfringe of  $1/T_T$ , which can be inferred from the temporal spacing between the two pulse parts at the same frequency.

At the propagation distance  $z_{T2} = 2 z_{T1}$  (panels 4),  $\omega_{T1-} = \omega_{T1+}$  and the spectrum has the same full width  $\omega_{T2+} - \omega_{T2-}$  as the initial spectrum, but now the negative frequencies are all contained in the leading edge of the pulse while the trailing edge contains only positive frequencies. The interference pattern is now much lessened. As the pulse further propagates in the nonlinear fibre (i.e., for  $z > z_{T2}$ ), the spectral brilliance at the central frequency drops down to zero (Fig. 3(a)), and the two parts of the spectrum separate in frequency, as demonstrated in [27, 28] where the spectral doubling of an optical signal by the SPM or cross-phase modulation phase shift generated by a triangular pulse has been investigated. A natural extension of this analysis would include the use of saw-tooth pulses, where the asymmetry of the intensity profile would cause one portion of the spectrum to evolve at a higher rate than the other [29]. We would like to emphasize that the spectral dynamics of the triangular pulse can be interpreted in terms of the well-known Fresnel bi-prism interference [30], which is widely taught in university textbooks [31, 32]. Indeed, taking advantage of the concept of space-time duality [33-35] and extending it to the frequency domain [7], the spectral interference pattern associated with the triangular pulse dynamics can be viewed as the spectral analogue of the spatial interference pattern that is observed after a bi-prism: similarly to the time-domain counterpart of the bi-prism experiment described in Ref. [36], the spectral interference pattern is localized with a bright fringe at the central frequency (see Fig. 2(c)).

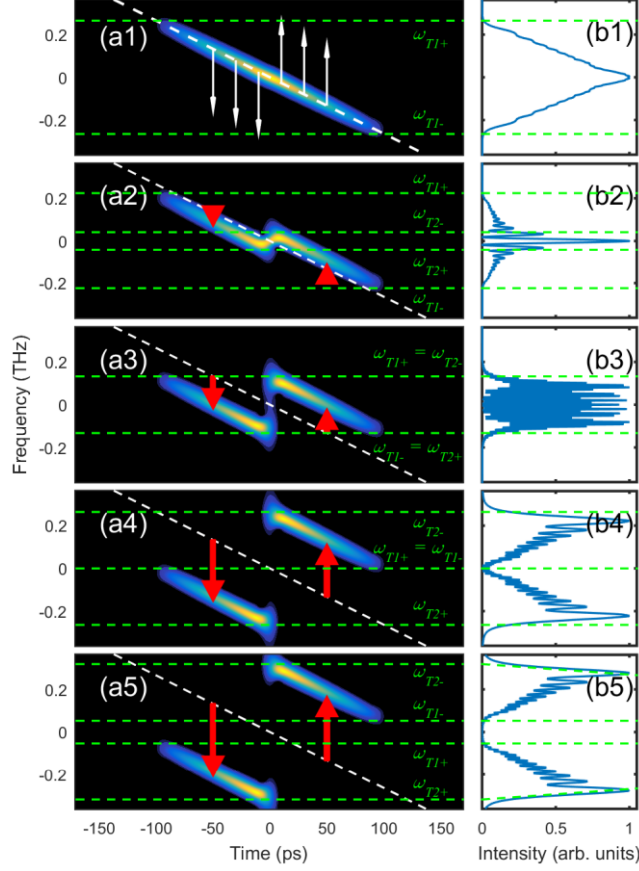


**Figure 7:** Spectro-temporal representation of a triangular pulse at different propagation distances in the fibre:  $z = 0$ ,  $z = 65$  m,  $z = z_{T1}$ ,  $z = z_{T2}$ , and  $z = 500$  m (panels 1 to 5, respectively). Subplots (a) and (b) show the spectrograms and the spectral intensity profiles, respectively. The white dashed lines represent the slope coefficient of the pulse chirp at the fibre input. The green dashed lines represent the theoretical predictions for  $\omega_{T1\pm}$  and  $\omega_{T2\pm}$ , respectively. The white arrows have a length proportional to the temporal gradient of the pulse intensity profile. The red arrows represent the frequency shifts experienced by the leading and trailing edges of the pulse  $\mp \gamma P z / T_T$ .

## 4. Results with realistic conditions

In the previous section, we have based our analysis on initially perfectly shaped pulses propagating in a purely nonlinear fibre. However, except for Gaussian waveforms, such ideal temporal profiles may be hard to generate. The goal of this section is to study the impact of realistic initial conditions of the input pulses and system parameters on the pulse evolution in the fibre. To this end, we have

generated the various input waveforms by the dispersive frequency-to-time mapping method that has been previously successfully used to synthesize high-quality parabolic pulses [12, 37, 38]. Within this approach, pulses with the desired temporal shape can be generated by shaping the pulse spectrum to be of the target waveform, followed by linear propagation in a second-order dispersive medium. In the far-field regime, the quadratic spectral phase imparted by dispersion onto the pulse translates into a quadratic temporal phase and, thus, the resulting temporal waveform is a scaled replica of the spectrum [38]. The small distortions of the temporal waveform generated by this approach lead to a degraded temporal gradient compared to the ideal case: the imperfect pulse shapes resulting from realistic conditions are presented as the dashed lines in Fig. 1 and may turn into phase fluctuations through SPM, as for instance has been pointed out in previous studies of chirped pulse amplification. Figure 8 summarizes the results obtained by this approach and accounting for the GVD of the HNLF. Given the strongly nonlinear regime of propagation, the fibre dispersion does not have a major impact on the spectral dynamics of the pulses. The use of a realistic initial condition of the input pulse does not bring about any significant qualitative difference in spectral dynamics with respect to the ideal case as for the super-Gaussian waveform is concerned. The dynamics of the parabolic shaped pulse are also qualitatively well reproduced with a realistic initial condition. However, the maximum spectral brilliance of the pulse is reduced to nearly a third of the value achieved in the ideal case, and the longitudinal evolution of the brilliance is not any longer symmetric with respect to the point of spectral focusing (blue dashed line in Fig. 3(a)). These observations are consistent with previous experiments where the maximum Strehl ratio measured did not exceed 0.6 [12]. Conversely, in the case of the triangular input pulse the dynamics are visibly impaired by the use of a realistic initial condition (Fig. 8(d)).

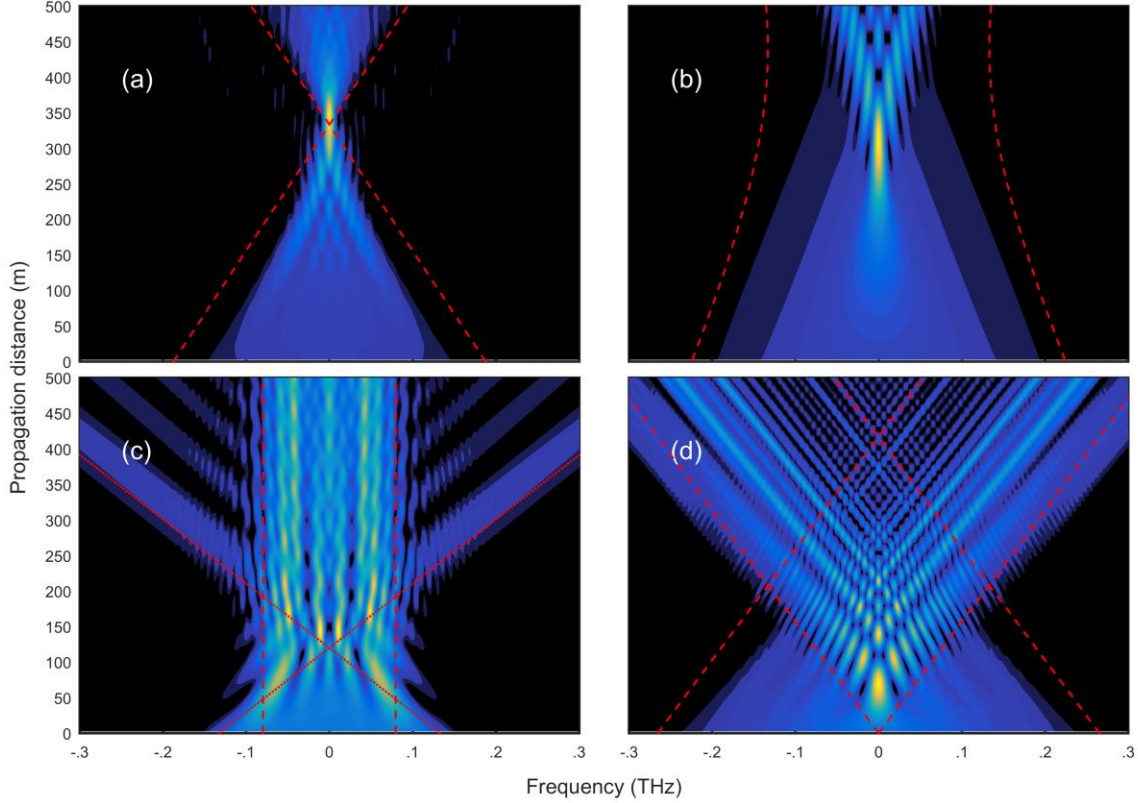


**Figure 8:** Longitudinal evolution of the spectra of frequency-to-time shaped (a) parabolic, (b) Gaussian, (c) fourth-order super-Gaussian, and (d) triangular incident pulses. The red dashed and dotted lines represent analytical predictions based on a simplified approach.

Once again, the use of spectrograms helps us elucidate the origin of the sensitivity of the triangular waveform to deviations from ideal shape. Indeed, while the chirp generated by SPM of an ideal triangular pulse has a discontinuity at the pulse center, the use of a realistic initial pulse shape results into a continuous temporal variation of the chirp, which now features a linear variation in the vicinity of  $t = 0$  between the two constant frequency offsets induced by SPM (Figs. 1 and 9). As a result of this, interference now develops between three different temporal portions of the pulse (panels 2 of Fig. 9), leading to a narrower central peak in the pulse spectrum with increased brilliance (Fig. 3(a)). Further, Fig. 9 highlights that for propagation in the fibre beyond  $z_{T2}$  when the two portions of the split spectrum separate in frequency in the ideal case, now energy remains always present in the central part of the spectrum, and as the temporal chirp near the pulse center evolves linearly, it contributes to the development of strong oscillations across the whole spectrum.

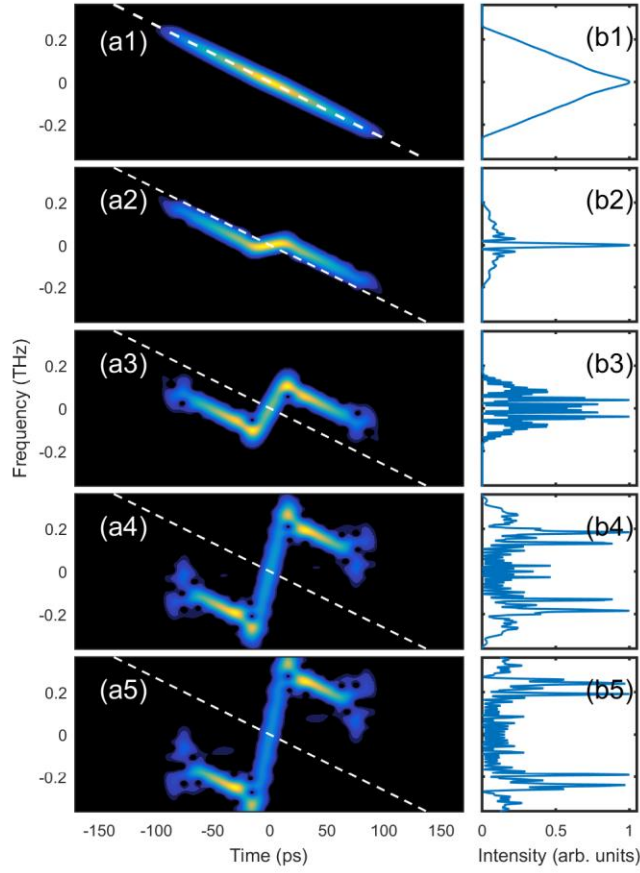


**Figure 9:** Spectro-temporal representation of a triangular pulse at different propagation distances in the fibre:  $z = 0$ ,  $z = 65$  m,  $z = z_{T1}$ ,  $z = z_{T2}$ , and  $z = 500$  m (panels 1 to 5, respectively). Subplots (a) and (b) show the spectrograms and the spectral intensity profiles, respectively.

## 5. Conclusion

We have studied the influence of the temporal intensity profile of the initial pulse on the process of spectral compression that occurs upon nonlinear propagation in an optical fibre. We have shown that necessary condition for nonlinear narrowing of the spectrum is that the input waveform can be fitted by a parabolic profile in its central part. Accordingly, neither super-Gaussian nor triangular pulses experience spectral narrowing while their nonlinear dynamics exhibit distinctly different features. The use of spectrograms helped us explain and predict in a simple manner the main trends observable in the evolution of the various incident waveforms. We have also emphasized that triangular pulses may lead to a spectral interference pattern very similar to the spatial interference that is observed in a Fresnel bi-prism experiment.

We believe that our results, obtained in the context of fibre optics, can be readily extended to highly nonlinear waveguides [9] to achieve on-the-chip functions. Moreover, we expect that the present study can support a better understanding of the practical tolerance of multistage fibre amplifier architectures to pulse degradation factors [39] as well as provide a deeper insight into the in-cavity dynamics of mode-locked fibre lasers [40, 41]. The proposed approach relying on time-frequency analysis can be naturally extended to the scenarios in which the temporal chirp and/or additional phase corrections [42] are applied to the propagating pulse by an external phase modulator [43] or through cross-phase modulation [44]. Lastly, we would like to note that recent experiments have shown that spectral compression is also relevant to quantum light [45].

## Acknowledgements

We acknowledge financial support by the Conseil Regional de Bourgogne (Pari Photcom) and the Agence Nationale de la Recherche (Labex ACTION program ANR-11-LABX-01-01).

## Appendix

Following the calculation described by S.C. Pinault and M. J. Potasek in Ref. [21], we derive an exact formula for the rms spectral width of an initially linearly chirped Gaussian pulse after undergoing SPM. The rms spectral width  $\sigma_\omega$  is defined as

$$\sigma_\omega^2 = \langle \omega^2 \rangle - \langle \omega \rangle^2 = \frac{\int \omega^2 |\tilde{\psi}(\omega)|^2 d\omega}{\int |\tilde{\psi}(\omega)|^2 d\omega} - \left[ \frac{\int \omega |\tilde{\psi}(\omega)|^2 d\omega}{\int |\tilde{\psi}(\omega)|^2 d\omega} \right]^2 \quad (1)$$

where  $\tilde{\psi}(\omega)$  is the Fourier transform of the pulse envelope  $\psi(t)$ . Using Fourier-transform and convolution theorems in a combination with integration by parts,  $\sigma_\omega^2$  can be expressed in terms of  $\psi(t)$  as [21]

$$\sigma_\omega^2 = \frac{\int |\psi'(t)|^2 dt}{\int |\psi(t)|^2 dt} + \left[ \frac{\int \psi'(t) \psi^*(t) dt}{\int |\psi(t)|^2 dt} \right]^2 \quad (2)$$

where ' and \* denote derivation and complex conjugation, respectively.

In the case of a chirped Gaussian pulse  $\psi(t) = \sqrt{P} \exp\left(-\frac{t^2}{2T_G^2}\right) \exp\left(-i\frac{At^2}{2} + i\phi_m e^{-\frac{t^2}{T_G^2}}\right)$ , where

$\phi_m = \gamma P z$  is the maximum nonlinear phase shift occurring at  $t = 0$ , the closed-form evaluation of the integrals above yields

$$\frac{\sigma_\omega}{\sigma_{\omega 0}} = \sqrt{1 + \frac{2\phi_m}{1 + A^2 T_G^4} \left( \frac{A T_G^2}{\sqrt{2}} + \frac{2\phi_m}{3\sqrt{3}} \right)}, \quad (3)$$

where  $\sigma_{\omega_0}$  is the initial rms spectral width of the chirped pulse.

Equation (3) can be used to draw some interesting conclusions. The kind of variation of  $\sigma_{\omega}$  over the fibre length depends on the initial chirp imposed on the pulse: while in the case of a positive chirp  $A > 0$ , the rms bandwidth of the pulse broadens monotonically with propagation distance, when  $A < 0$ , the bandwidth first narrows, reaching a minimum at the propagation distance

$$z_{\sigma} = -\frac{3}{4} \sqrt{\frac{3}{2}} \frac{A T_G^2}{\gamma P} \quad (4)$$

Using this result in Eq. (3), we obtain a maximum rms spectral compression ratio given by

$$(C_{rms})_{\max} = \left( 1 - \frac{3\sqrt{3}}{8} \frac{A^2 T_G^4}{1 + A^2 T_G^4} \right)^{\frac{1}{2}} \quad (5)$$

We can see that for large values of the product  $A T_G$ ,  $(C_{rms})_{\max}$  approaches a constant value

$$(C_{rms})_{\max} \approx \left( 1 - \frac{3\sqrt{3}}{8} \right)^{\frac{1}{2}} \approx 1.69 \text{ independent of the input pulse parameters.}$$

## References

- [1] R.H. Stolen, C. Lin, Self-phase modulation in silica optical fibers, Phys. Rev. A, 17 (1978) 1448-1453.
- [2] A.V. Zohrabian, L.K. Mouradian, Compression of the spectrum of picosecond ultrashort pulses, Quantum Electron., 25 (1995) 1076.
- [3] M. Oberthaler, R.A. Höpfel, Spectral narrowing of ultrashort laser pulses by self-phase modulation in optical fibers, Appl. Phys. Lett., 63 (1993) 1017-1019.
- [4] S.A. Planas, N.L. Pires Mansur, C.H. Brito Cruz, H.L. Fragnito, Spectral narrowing in the propagation of chirped pulses in single-mode fibers, Opt. Lett., 18 (1993) 699-701.
- [5] B.R. Washburn, J.A. Buck, S.E. Ralph, Transform-limited spectral compression due to self-phase modulation in fibers, Opt. Lett., 25 (2000) 445-447.

- [6] D.A. Sidorov-Biryukov, A. Fernandez, L. Zhu, A. Pugzlys, E.E. Serebryannikov, A. Baltuska, A.M. Zheltikov, Spectral narrowing of chirp-free light pulses in anomalously dispersive, highly nonlinear photonic-crystal fibers, *Opt. Express*, 16 (2008) 2502-2507.
- [7] E.R. Andresen, C. Finot, D. Oron, H. Rigneault, Spectral Analog of the Gouy Phase Shift, *Phys. Rev. Lett.*, 110 (2013) 143902.
- [8] E.R. Andresen, J. Thogersen, S.R. Keiding, Spectral compression of femtosecond pulses in photonic crystal fibers, *Opt. Lett.*, 30 (2005) 2025-2027.
- [9] C. Mei, J. Yuan, K. Wang, X. Sang, C. Yu, Chirp-free Spectral Compression of Parabolic Pulses in Silicon nitride Channel Waveguides, 21st Optoelectronics and Communications Conference / International Conference on Photonics in Switching, Japan, 2016, pp. WE1-5.
- [10] M. Rusu, O.G. Okhotnikov, All-fiber picosecond laser source based on nonlinear spectral compression, *Appl. Phys. Lett.*, 89 (2006) 091118.
- [11] J.P. Limpert, T. Gabler, A. Liem, H. Zellmer, A. Tünnermann, SPM-induced spectral compression of picosecond pulses in a single-mode Yb-doped fiber amplifier, *Appl. Phys. B*, 74 (2002) 191-195.
- [12] J. Fatome, B. Kibler, E.R. Andresen, H. Rigneault, C. Finot, All-fiber spectral compression of picosecond pulses at telecommunication wavelength enhanced by amplitude shaping, *Appl. Opt.*, 51 (2012) 4547-4553.
- [13] C. Bao, X. Xiao, C. Yang, Spectral compression of a dispersion-managed mode-locked Tm: fiber laser at 1.9  $\mu\text{m}$ , *IEEE Photon. Technol. Lett.*, 28 (2015) 497-500.
- [14] S. Wang, W. Chen, P. Qin, Y. Song, M. Hu, B. Liu, Spectral and temporal breathing self-similar evolution in a fiber amplifier for low-noise transform-limited pulse generation, *Opt. Lett.*, 41 (2016) 5286-5289.
- [15] E.R. Andresen, J.M. Dudley, C. Finot, D. Oron, H. Rigneault, Transform-limited spectral compression by self-phase modulation of amplitude shaped pulses with negative chirp, *Opt. Lett.*, 36 (2011) 707-709.
- [16] C. Finot, F. Parmigiani, P. Petropoulos, D.J. Richardson, Parabolic pulse evolution in normally dispersive fiber amplifiers preceding the similariton formation regime, *Opt. Express*, 14 (2006) 3161-3170.
- [17] C. Finot, S. Boscolo, Design rules for nonlinear spectral compression in optical fibers, *J. Opt. Soc. Am. B*, 33 (2016) 760-767.

- [18] G.P. Agrawal, *Nonlinear Fiber Optics*, Fourth Edition, Academic Press, San Francisco, CA, 2006.
- [19] A. Maréchal, Etude des effets combinés de la diffraction et des aberrations géométriques sur l'image d'un point lumineux, *Rev. Opt.*, 2 (1947) 257-277.
- [20] D.N. Schimpf, E. Seise, J. Limpert, A. Tünnermann, Self-phase modulation compensated by positive dispersion in chirped-pulse systems, *Opt. Express*, 17 (2009) 4997-5007.
- [21] S.C. Pinault, M.J. Potasek, Frequency broadening by self-phase modulation in optical fibers, *J. Opt. Soc. Amer. B*, 2 (1985) 1318-1319.
- [22] E.B. Treacy, Measurement and Interpretation of Dynamic Spectrograms of Picosecond Light Pulses, *Journal of Applied Physics*, 42 (1971) 3848-3858.
- [23] J. Azana, Time-frequency (Wigner) analysis of linear and nonlinear pulse propagation in optical fibers, *EURASIP Journal on Applied Signal Processing*, 10 (2005) 1554-1565.
- [24] S. Linden, H. Giessen, J. Kruhl, XFROG - A new method for amplitude and phase characterization of weak ultrashort pulses, *Phys. Stat. Sol.*, 206 (1998) 119-124.
- [25] C. Cheng, Y. Wang, Y. Ou, Q. Lv, Transform-Limited Spectral Compression by Using Negatively Chirped Parabolic Pulse in All-Normal Dispersion Photonic Crystal Fibers, *J. Nonlinear Opt. Phys. Mater*, 21 (2012) 1250040.
- [26] D. Anderson, M. Lisak, Analytic study of pulse broadening in dispersive optical fibers, *Phys. Rev. A*, 35 (1987) 184-187.
- [27] A. Latkin, S. Boscolo, R.S. Bhamber, S.K. Turitsyn, Doubling of optical signals using triangular pulses, *J. Opt. Soc. Am. B*, 26 (2009) 1492-1496.
- [28] N. Verscheure, C. Finot, Pulse doubling and wavelength conversion through triangular nonlinear pulse reshaping, *Electron. Lett.*, 47 (2011) 1194-1196.
- [29] F. Parmigiani, M. Ibsen, T.T. Ng, L. Provost, P. Petropoulos, D.J. Richardson, An efficient wavelength converter exploiting a grating based saw-tooth pulse shaper, *IEEE Photon. Technol. Lett.*, 20 (2008) 1461-1463.
- [30] *Œuvres complètes d'Augustin Fresnel*, Imprimerie impériale, Paris, 1866-1870.
- [31] E. Hecht, *Optics*, 4th, International edition, Addison-Wesley, San Francisco, (2002).
- [32] M. Born, E. Wolf, *Principles of Optics*, Seventh Edition ed., Cambridge University Press 1999.

- [33] P. Tournois, J. Vernet, G. Biennu, Sur l'analogie optique de certains montages électroniques: Formation d'images temporelles de signaux électriques, CR Acad. Sci, 267 (1968) 375-378.
- [34] R. Salem, M.A. Foster, A.L. Gaeta, Application of space-time duality to ultrahigh-speed optical signal processing, *Advances in Optics and Photonics*, 5 (2013) 274-317.
- [35] B.H. Kolner, Space-time duality and the theory of temporal imaging, *IEEE J. Quantum Electron.*, 30 (1994) 1951-1963.
- [36] F. Chaussard, H. Rigneault, C. Finot, Two-wave interferences space-time duality: Young slits, Fresnel biprism and Billet bilens, *Opt. Commun.*, in press (2017).
- [37] D.N. Schimpf, J. Limpert, A. Tünnermann, Controlling the influence of SPM in fiber-based chirped-pulse amplification systems by using an actively shaped parabolic spectrum, *Opt. Express*, 15 (2007) 16945-16953.
- [38] J. Huh, J. Azaña, Generation of high-quality parabolic pulses with optimized duration and energy by use of dispersive frequency-to-time mapping, *Opt. Express*, 23 (2015) 27751-27762.
- [39] D.A. Korobko, O.G. Okhotnikov, I.O. Zolotovskii, Multistage fiber preamplifier comprising spectral compression for generation of high-energy laser pulses *J. Opt. Soc. Am. B*, 33 (2016) 239-245.
- [40] S. Boscolo, S.K. Turitsyn, C. Finot, Amplifier similariton fiber laser with nonlinear spectral compression, *Opt. Lett.*, 37 (2012) 4531-4533.
- [41] Y. Lan, Y. Song, M. Hu, B. Liu, L. Chai, C. Wang, Enhanced spectral breathing for sub-25 fs pulse generation in a Yb-fiber laser, *Opt. Lett.*, 38 (2013) 1292-1294.
- [42] S. Boscolo, L.K. Mouradian, C. Finot, Enhanced nonlinear spectral compression in fibre by external sinusoidal phase modulation, *J. Opt.*, 18 (2016) 105504.
- [43] B.W. Plansinis, W.R. Donaldson, G.P. Agrawal, Spectral changes induced by a phase modulator acting as a time lens, *J. Opt. Soc. Am. B*, 32 (2015) 1550-1554.
- [44] L.W. Guo, C.H. Zhou, Spectral narrowing of negatively chirped femtosecond pulse by cross-phase modulation in a single-mode optical fiber, *Opt. Commun.*, 260 (2006) 140-143.
- [45] M. Karpiński, M. Jachura, L.J. Wright, B.J. Smith, Bandwidth manipulation of quantum light by an electro-optic time lens, *Nat Photon*, advance online publication (2016).